



Energy Power Spectra Measured at an Interplanetary Shock by the New Horizon's SWAP Experiment: 1D Full Particle Simulations versus Observations

Bertrand Lembège¹ , Zhongwei Yang^{1,2,3,4} , and Gary P Zank^{5,6}

¹ LATMOS -IPSL-CNRS, Guyancourt 78280, France; bertrand.lembège@latmos.ipsl.fr

² Key Laboratory of Earth and Planetary Physics, Institute of Geology and Geophysics, CAS, Beijing, 100029, People's Republic of China; yangz@latmos.ipsl.fr

³ Innovation Academy for Earth Environment, CAS, Beijing, 100029, People's Republic of China

⁴ CAS Key Laboratory of Geospace Environment, Chinese Academy of Sciences, Department of Geophysics and Planetary Science, University of Science and Technology of China, Hefei 230026, People's Republic of China

⁵ Center for Space Plasma and Aeronomic Research (CSPAR), University of Alabama in Huntsville, Huntsville, AL 35805, USA; garyp.zank@gmail.com

⁶ Department of Space Science, University of Alabama in Huntsville, Huntsville, AL 35899, USA

Received 2019 October 13; revised 2019 December 19; accepted 2019 December 23; published 2020 February 11

Abstract

One-dimensional particle-in-cell (PIC) simulations are used to analyze the energy spectra measured by the *New Horizons*' Solar Wind Around Pluto (SWAP) instrument in the upstream region of an interplanetary shock observed at a distance of ~ 34 au from the Sun. The use of individual populations simulating the different solar wind ion and pick-up ion (PUI) populations allows us to clearly identify the contribution of each population to the global energy spectra. The important role of shock front obliquity is stressed in the formation of PUIs streaming back along the magnetic field into the upstream region far from the front. Energy spectra measured by the SWAP experiment are well reproduced in the present simulations. A detailed analysis shows that (1) the highest-energy part of the spectrum is formed primarily by both backstreaming PUI- H^+ and PUI- He^+ ; (2) the middle-energy part of the energy spectrum is composed of both solar wind SW- H^+ and SW- He^{2+} incoming ions that are superimposed on the PUI- H^+ population; and (3) the low-energy range is composed of incoming PUI- H^+ . The agreement between experimental and simulation results is improved by using an initially filled-shell distribution for the PUI- H^+ population (instead of a zero-thickness shell), as this affects the low-energy part of the spectrum strongly. This means that PUI- H^+ ions have sufficient time to diffuse onto and fill out a shell distribution after their initial pick-up in the heliosphere, indicating that the subsequent cooling has an important impact on the global energy spectrum.

Unified Astronomy Thesaurus concepts: Heliosphere (711); Interplanetary shocks (829); Space plasmas (1544); Interplanetary particle acceleration (826)

1. Introduction

As the solar wind (SW) expands radially outward from the Sun, slow interstellar neutral atoms flow into the heliosphere and interact with SW ions via charge exchange (Zank 1999, 2015). The newborn ionized interstellar pick-up ion (PUI) immediately starts to gyrate around the interplanetary magnetic field (IMF) and is accelerated by the motional electric field of the SW; hence the term “PUIs.” Typically, depending on the orientation of the IMF with respect to the inflowing neutral atoms (primarily H and a smaller fraction of neutral He), the continued ionization of neutral interstellar atoms and their random gyrophase initially leads to the formation of a ring-beam distribution of PUIs. The formed PUI velocity distribution differs from that of the core SWI population, and PUIs have a range of velocities that extends from zero (their initial neutral flow speed) to twice the SWI velocity in the SW reference frame, depending on the phase of their gyromotion. The ring-beam distribution is unstable, and PUIs scatter in both pitch angle and velocity space due to the effects of both preexisting SW turbulence and waves triggered by the microinstabilities associated with the unstable distribution. The scattering results in the formation of an isotropic shell distribution. As the shell is advected outward from the Sun, the PUIs adiabatically cool, resulting in a filled-shell distribution with older PUIs inside the outermost shell as new PUIs are scatter onto the outer shell of the distribution. Indeed, this basic transport process is observed by the *New Horizons*'s SWAP instrument in its measurements of both the basic PUI and SW

plasma moment-integrated distributions and well described theoretically (Zank et al. 2018). Zhao et al. (2019) have further extended these moment-integrated transport results to the filled-shell PUI distribution function itself, including the PUI heat flux induced by the turbulent scattering of PUIs.

The *New Horizons*'s (NH) mission was launched on 2006 January 19, and completed its Pluto encounter during 2015 July. The NH SWAP (SW Around Pluto) instrument is a top-hat analyzer that detects ions in the energy range $0.035 \sim 7.5 \text{ keV } q^{-1}$ (McComas et al. 2008; Elliott et al. 2016). SWAP has made high-resolution measurements of SW ions to at least 41 au from the Sun (McComas et al. 2017) and corresponding high-resolution measurements of the PUI velocity distribution, thanks to its large field of view. SWAP has made direct measurements of interstellar PUI- H^+ and PUI- He^{2+} components (McComas et al. 2017) comoving with the SW out from 22 to 38 au. Figure 1(a) is an example of the energy spectrum observed by the SWAP experiment at 25.7 au (McComas et al. 2017), where data were accumulated over a 24 hr period.

Observations of both PUI- He^{2+} and PUI- H^+ at an interplanetary (IP) shock in the environment of Pluto at 34 au were described recently by Zirnstein et al. (2018). A striking observation made by SWAP was the discovery of a tail in the PUI distribution downstream of the shock for energies above the PUI- H^+ cutoff. Typical measurements are shown in Figure 1(b) (Zirnstein et al. 2018). Upstream of the shock

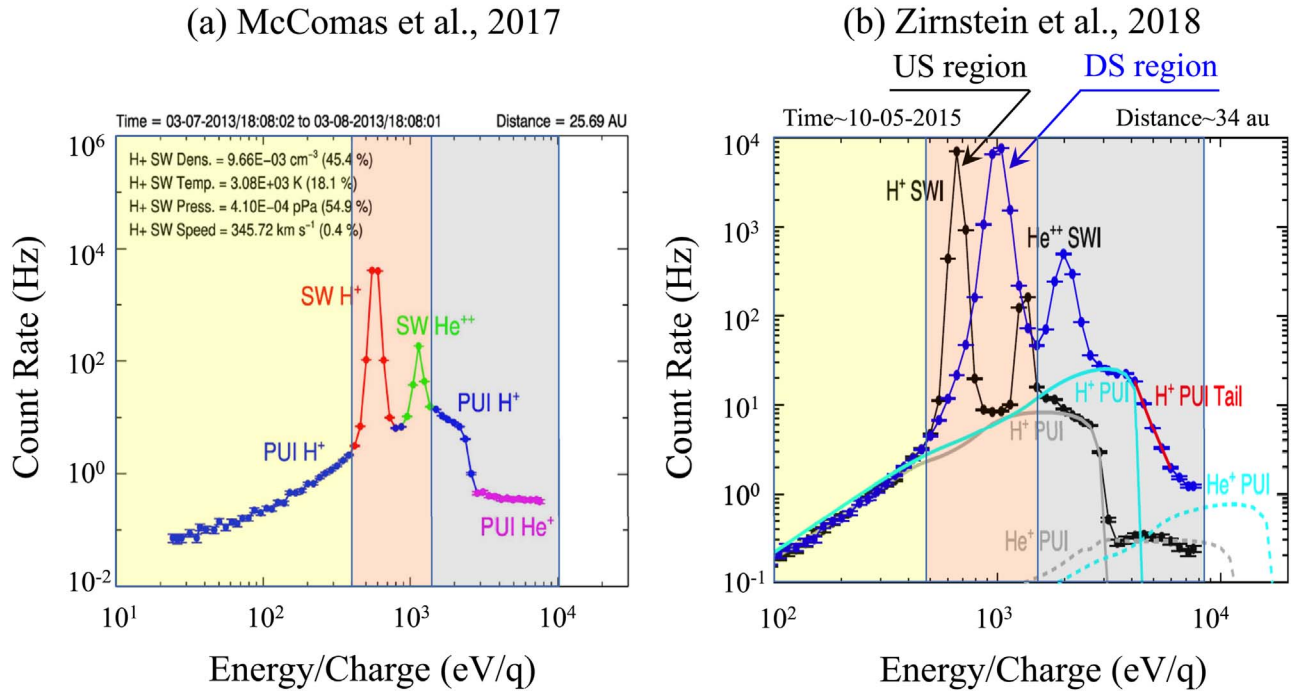


Figure 1. Panel (a) shows a typical example of a SWAP energy spectrum measured at 25.7 au, color coded with the primary source of the counts: solar wind ions (SWIs) and interstellar pick-up ions (PUIs). Observations were collected over one day, and provide highly statistically significant measurements (from McComas and al., 2017). Three energy ranges are identified in the spectrum by the vertical colored areas (see the corresponding text). Panel (b) shows another observation collected by the SWAP instrument before (black) and after (blue) the crossing of an interplanetary shock by *New Horizons* that was measured near Pluto at 34 au. Fits to the PUI- H^+ before (gray) and after (blue) the shock front are shown, respectively, based on the models of Vasyliunas & Siscoe (1976) and Zank et al. (1996, 2010) (from Zirnstein et al. 2018). “US” and “DS” refer to upstream and downstream regions of the shock, respectively.

front, the SW- H^+ and the SW- He^{2+} (twice the energy per charge) ions, are relatively cold, and the PUI- H^+ ions are clearly identified, but there a tail population is also present at energies above the PUI- H^+ cutoff, which was not included in previous models. On comparing the energy spectra of Figure 1(a) (measured in the SW) and those in the upstream region of the IP shock in Figure 1(b), a very strong similarity is seen. Instead of attempting to derive the best fit from previous models that describe the upstream region (Vasyliunas & Siscoe 1976), and the DS region (Zank et al. 1996, 2010), in as in Figure 1(b), we divide the entire energy range into three parts: a low (yellow), middle (pink), and high (gray) energy range corresponding respectively to PUI- H^+ , the SW ion populations (both SW- H^+ and SW- He^{2+}), and both PUI- He^+ and PUI- H^+ populations. Three different vertical colored bars identify these ranges, respectively. In the present paper, we focus on these energy spectra to address three primary questions: (1) can we retrieve the energy spectrum defined within each energy range from the simulations; (2) what is the contribution of each population to the full energy range, and to each energy range; and finally (3) what is the origin of the high-energy ions (above the SW- He^{2+} energy cutoff) in the upstream region of the IP shock?

2. Numerical Simulation Conditions

To answer the above questions, we use a 1D full electromagnetic particle-in-cell (PIC) code named Epoch (Arber et al. 2015) to simulate the interaction of the SW with a supercritical, collisionless, interplanetary shock propagating within a quasi-perpendicular angular range. The shock is produced by the injection method as in previous PIC simulations (Lee et al. 2005; Matsukiyo et al. 2007;

Yang et al. 2015; Lembège & Yang 2016, 2018). To reproduce self consistently the affect of PUIs and SW ions, five particle species are introduced within our PIC code: three solar wind populations (electrons, SW- H^+ and SW- He^{2+} ions) and two pick-up populations (PUI- H^+ and PUI- He^+). All particles are injected from the left side of the simulation box with an inflow upstream drift speed, V_{inj} , and are reflected at the other end (the reflecting wall). The shock front builds up (as incoming/reflected plasmas interact) and moves with a speed V_{ref} from the right to the left along the $-x$ axis. The initial distribution functions for the SW ions and electrons are Maxwellian. PUIs are distributed on a zero-thickness sphere (unless indicated differently) in velocity space centered at V_{inj} with radius V_{shell} as in earlier works (Lipatov & Zank 1999; Lee et al. 2005; Matsukiyo & Scholer 2011; Oka et al. 2011; Yang et al. 2012a; Kumar et al. 2018). The spatial resolution $dx = 0.005 d_i$ and the temporal resolution is given by $dt = 1.5 e-4 \omega_{ci}^{-1}$; the units of velocity, spatial length, and time are the Alfvén velocity, V_A , the ion inertial length, d_i defined in the upstream region ($=c/w_{pi}$) and the inverse ion gyrofrequency, ω_{ci}^{-1} , respectively. The initial injection-bulk velocity of the upstream plasma is $V_{inj} = 7 V_A$. The upstream Alfvén Mach number of the shock is $M_A = (V_{inj} + V_{ref})/V_A$, where the Alfvén speed V_A is equal to 1. The ambient magnetic field B_0 lies in x - y plane, and the shock normal angle $\theta_{Bn}(=55^\circ)$ is defined between B_0 and the $-x$ axis. All basic parameters are as follows: plasma box size length $L_x = 2100 c/\omega_{pi}$; Mach number $M_A = 9-11$; light velocity $c = 30$; mass ratio $m_i/m_e = 100$; and the electron plasma to cyclotron frequency ratio $\omega_{pe}/\Omega_{ce} = 3$. The SW and pick-up plasma parameters are chosen to be as similar as possible to the local plasma conditions in the Pluto environment observed by SWAP (Zirnstein et al. 2018), shown in

Table 1
Values of Upstream Plasma Parameters Used in the Simulations

Parameter	Description	Electrons	SWIs	PUIs
$v_{th,x,y,z}$	Thermal velocity	5.0	0.14	Shell distribution
λ_D	Debye length	0.017	0.0047	
ρ_c	Gyro-radius	0.05	0.14	
c/ω_p	Inertial length	0.1	1	
ω_c	Gyrofrequency	100	1	
ω_p	Plasma frequency	300	30	
τ_c	Gyroperiod	0.01	1	
β	Plasma beta	0.5	0.04	

Table 1. The ion plasma beta is assumed to be $\beta_i = 0.04$ (the ratio of the ion kinetic pressure to the magnetic pressure), while the electron plasma beta $\beta_e = 0.5$ is chosen as in previous PIC simulations. Initially, 200 particles for each species are used in a cell. The upstream plasma is quasi-neutral, i.e., $n_e = n_i$, where $n_i = n_{SWI} + n_{PUI} = N_{SWI} \times SWI\% + N_{PUI} \times PUI\%$, where n_e , n_i , n_{SWI} and n_{PUI} are the densities of the electrons (subscript “e”), of the total ions (subscript “i”), of the SW ions (subscript “SWI”), and of the PUIs (subscript “PUI”), respectively. N_{SWI} , N_{PUI} , $SWI\%$, and $PUI\%$ are the counts of each ionic species and their relatively weighted percentage in the PIC simulation, respectively. We use the following percentage ratios, $SWI\text{--}He^{2+}/SWI\text{--}H^+ = 4\%$, and $PUI\text{--}H^+/SWI\text{--}H^+ = 4\%$, which approximate the observed conditions. The percentage of $PUI\text{--}He^+/SWI\text{--}H^+ = 0.8\%$ is so low that $PUI\text{--}He^+$ can be treated as test particles, which saves computer time.

3. Simulation Results

3.1. Affect of Backstreaming PUIs on the Total Energy Spectra

A simple way to observe energetic particles upstream of a shock front is to consider an oblique (quasi-perpendicular) shock, as a certain percentage of the incoming ions interact with the shock front, at which they are reflected and then stream far upstream into the SW. A numerical parametric analysis has been performed to determine the appropriate conditions (in terms of the Alfvén Mach number M_A regime and obliquity of the shock front) to produce a noticeable number of backstreaming ions. Note that the energetic ions in the SWAP observed spectra (above the $SWI\text{--}He^{2+}$ energy cutoff) correspond to PUI populations (and not to SW ions). In the present results, we mainly focus on a single reference simulation for a shock with $M_A = 9\text{--}11$ and $\theta_{Bn} = 55^\circ$. The results are shown in Figure 2. A two-step technique is used to identify the backstreaming ions: first, we separate the incident ions into two groups, those that are reflected and those that are directly transmitted at the shock front, as in previous work (Yang et al. 2012b); second, we keep track of all reflected ions until the end of the simulation. If a reflected ion has a parallel velocity directed upstream and is never advected downstream, the particle will be selected as a backstreaming ion.

The main field components are shown in Figure 2(a). Figures 2(b)–(f) show electron phase space and ion phase space (x, v_{\parallel}) plots, where the velocity component v_{\parallel} is calculated with respect to the local \mathbf{B} field. These results clearly show the formation of backstreaming PUIs for both $PUI\text{--}H^+$ and $PUI\text{--}He^+$ (Figures 2(e) and (f)). The simulation box ($L_x = 2100 c/\omega_{pi}$) and the time length of the run ($T_{end} = 150\Omega_{ci}^{-1}$, where Ω_{ci} denotes the proton cyclotron frequency) have been chosen to be sufficiently

long to ensure a well-matured shock front and to follow all populations interacting with the shock front, including in particular the heavy ions He^+ and He^{2+} . In contrast, no backstreaming SW ions are observed in Figures 2(c) and (d). The modulation observed in the upstream region of the SW ions is due to a two-stream type instability excited between the incoming/reflected PUIs populations. The reasons for the absence of backstreaming SW ions, the acceleration mechanism responsible for the formation of backstreaming PUIs and the precise identification of the two-stream instabilities are beyond the scope of the present paper and will be analyzed in a separate study (see Zank et al. 1996 for a related theoretical analysis). Figure 2(g) shows how the density decreases with distance from the shock front for each backstreaming PUI population.

Figure 3 shows the energy spectra measured within a large sampling box ($\Delta x = 300 c/\omega_{pi}$) illustrated by a red rectangle superimposed in the particle phase space (x, v_{\parallel}) of Figure 2. The sampling box is located at an upstream distance of $20 c/\omega_{pi}$ from the ramp. Figure 3(a) shows the global spectrum which can be directly compared with the observations shown in Figure 1(a) (or the observations measured in the upstream region of the IP shock shown in Figure 1(b)). Figure 3(b) shows the contribution of each of the five populations to the global or total spectrum (where incoming and backstreaming ions are not separated, but are all included without distinction). Figure 3(c) shows the contribution of each subpopulation to the global distribution (where incoming and backstreaming ions are separated). Red and blue colored curves distinguish H^+ and heavy ions (He^+ and He^{2+}), respectively. Let us remind that the power spectra have been estimated over a large size of the sampling box to approach “as much as possible” the 24h averaged measurement made by SWAP. Different tests have been made with different sizes of the sampling box that show that a box size larger than $300 c/\omega_{pi}$ does not bring any change in the energy spectra. Moreover, the time length of the simulation is very large ($150 \omega_{ci}^{-1}$), so that the dynamics of the shock front and the measurement made in the upstream region are totally independent of and far from the initial conditions.

Good agreement is found between observations and the simulation results, which is clear in terms of the global spectrum and the identification of the three main energy ranges (Figures 3(c) and 1). By distinguishing between the incoming and backstreaming subpopulations, we determine clearly which population contributes to each of the three energy ranges. (1) We find that the low-energy range (yellow) is made up primarily of incoming $PUI\text{--}H^+$. (2) The middle-energy range (pink) is comprised of SW ions populations that are superimposed on the incoming $PUI\text{--}H^+$. (3) The high-energy range (above the SW ion cutoff) is more complicated. To clarify the spectral structure of this energy regime, four successive cutoffs can be defined (as energy increases), illustrated by the vertical dashed lines in Figure 3(c). Here, “c1” is the cutoff for the incoming $PUI\text{--}H^+$, “c2” that of the incoming $PUI\text{--}He^+$, “c3” for the BS- $PUI\text{--}H^+$, and “c4” for BS- $PUI\text{--}He^+$. Note that the cutoff “c2” allows us to separate the $PUI\text{--}He^+$ population into two parts, namely the incoming and the backstreaming $PUI\text{--}He^+$. Similarly, the cutoff “c1” separates the same $PUI\text{--}H^+$ population into incoming and backstreaming $PUI\text{--}H^+$. This approach allows us to determine more simply what population contributes to what part of the spectrum above the SW ion cutoff. There is some interplay and movement of particles from one to another of the four subpopulations within the high-energy range (between “c1”

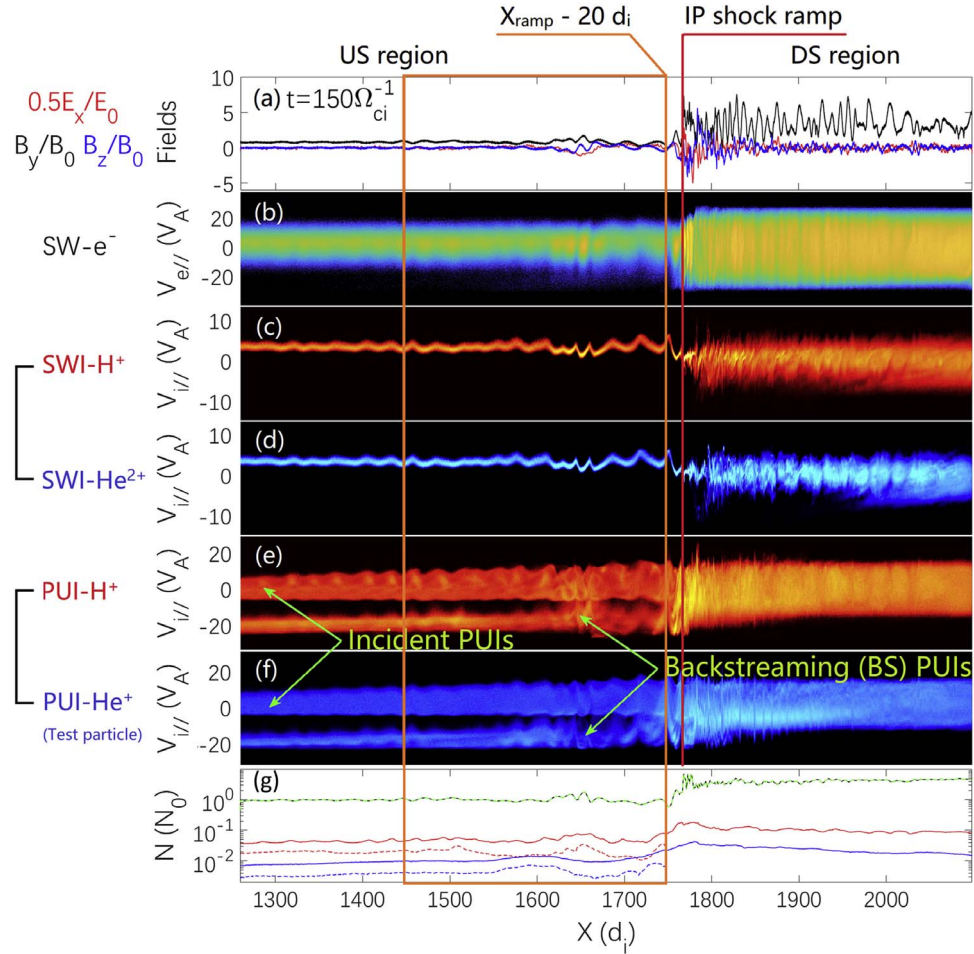


Figure 2. Top plot (a) shows magnetic field profiles B_y (black) and B_z (blue), and the electric field component E_x (red) at a late time $t = 150 \Omega_{ci}^{-1}$ of the simulation. The plots below show the phase space ($x, v_{//}$) for the different populations: (b) electrons; (c) SW- H^+ ions; (d) SW- He^{2+} ions; (e) PUI- H^+ ; (f) PUI- He^+ ; the parallel velocity component ($v_{//}$) is defined with respect to the local magnetic field; and (g) density profiles of PUI- H^+ and PUI- He^+ ions are indicated by red and blue solid curves, respectively. The density profiles of corresponding BS ions are represented by dashed (red and blue) curves. The total ion density (dotted black), and the electron density (green) are also shown for reference. The vertical red line identifies the ramp location in the shock front. The large colored rectangle ($\Delta x = 300 c/\omega_{pi}$) is located at a distance of $20 c/\omega_{pi}$ from the ramp and identifies the upstream sampling x -range where the energy spectra are calculated (see Figures 3–5).

and “c4”), depending on the different plasma conditions (upstream plasma β , M_A regime, shock obliquity). This can lead to different spectral shapes within the high-energy range. This will be further analyzed in a separate study. Note that the high-energy range is carried by backstreaming ions of both PUI populations only (each having its own cutoff) and not backstreaming SW ions.

Further analysis of the simulation and observed spectra reveals some differences. In particular, (1) in the low-energy range, the shoulder decreases strongly in Figure 3(a), but smoothly in Figure 1 when approaching very low-energy values and (2) there is a difference in the high-energy range between the observations and the simulation results. These differences are investigated further below.

3.2. Affect of Using a PUI- H^+ Shell

The spectra of Figure 3 were obtained using a zero-thickness shell model for both the PUI- H^+ and PUI- He^+ populations. This, however, neglects the effects of adiabatic cooling after a PUI was created. Because the low-energy range of the total spectrum is determined mainly by the PUI- H^+ (Figure 1), we can anticipate that the adiabatically cooled PUIs may contribute to this part of the spectrum. We therefore replace the

zero-thickness shell by a filled-in shell for the PUI- H^+ population only, and perform a separate simulation run. The form of the filled-in shell distribution in the upstream plasma rest frame is similar to that used in Equation (1) of Burrows et al. (2010); namely, $F(v) = A_0(v/u)^{-3/2} \exp[-1/r (v/u)^{-3/2}]$, $A_0 (=0.18)$ is a constant, ionization cavity $1/r = 6/90$, v is the pick-up particle velocity, and u is the maximum value of the velocity shell radius ($10V_A$ is used based on the shock speed). The filled-in shells are constructed by viewing them as a collection of concentric shell distributions as detailed in Williams & Zank (1994) and Zank (1999). The resulting energy spectra are shown in Figures 4(a) and (c) at time $t = 0$ (used as a reference time) and in Figures 4(b) and (d) at time $t = 150 \Omega_{ci}^{-1}$, respectively. The conditions under which the spectra are derived are identical for both simulations, i.e., the sampling box (width of $\Delta x = 300 c/\omega_{pi}$) is located at a distance of $20 c/\omega_{pi}$ from the shock ramp (see Figure 2 for reference). The spectra are presented using the same scales for a direct quantitative comparison. The main results for the filled-shell case at $t = 150 \Omega_{ci}^{-1}$ are summarized as follows:

(1) Very good agreement between simulation and observation is now found for the low-energy regime (yellow area in Figure 4(d)) (see Figure 1). This is easily understood by noting

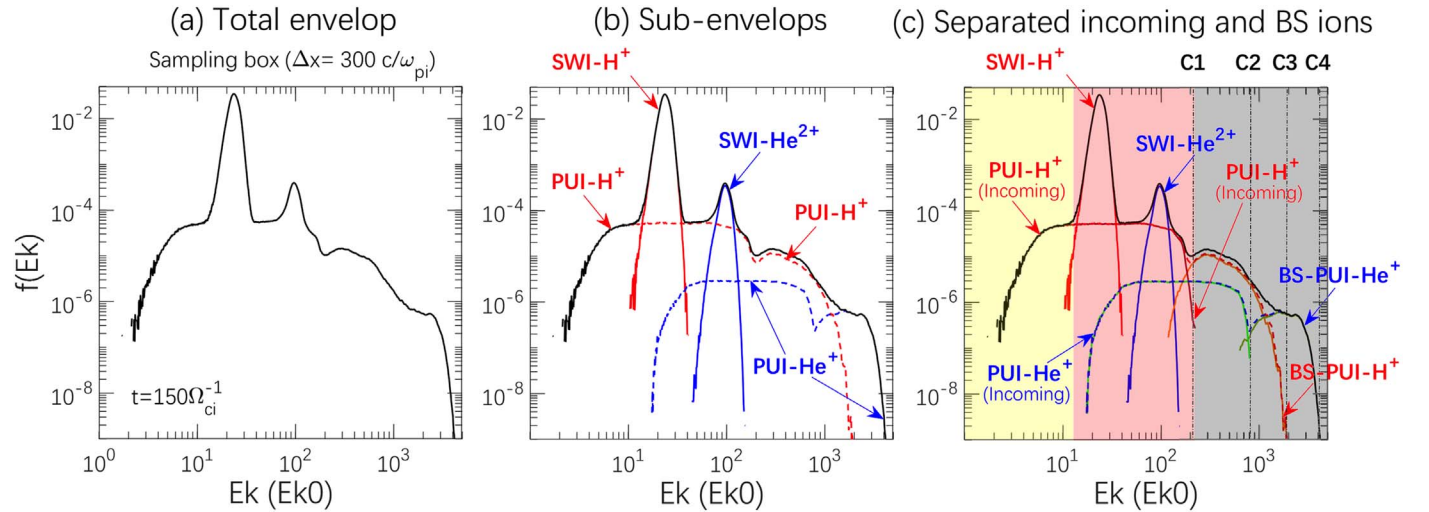


Figure 3. (a) Distribution for the total energy spectrum derived within the sampling range $\Delta x = 300 c/\omega_{pi}$ at a late time $t = 150 \Omega_{ci}^{-1}$ of the simulation (see Figure 2); (b) the same result, but now identifying the subspectra corresponding to each of the four different ion populations (incoming and backstreaming PUIs are not yet separated); (c) the same results but where now individual energy spectra are identified for each of the six populations (four incoming ion and two backstreaming ion populations, and the incident and backstreaming PUI contributions are now separated). The red and blue colored curves are used for H^+ and heavy ions (He^+ and He^{2+}), respectively.

that in the solar wind $PUI-H^+$ has enough time to scatter in pitch angle and velocity space (due to the intrinsic turbulence of the expanding solar wind; see Zank et al. 2018) to cool adiabatically and fill in the shell. This result also shows that the generation of upstream waves by a two-stream type instability between incident/backstreaming populations (Figures 2(b)–(f)) is insufficient to strongly scatter and diffuse the PUIs and to fill in the initial zero-thickness shell.

(2) A main peak now forms in the spectral region corresponding to incident $PUI-H^+$ (being superimposed on $SW-H^+$ ions) in contrast to observational results that show such a maximum is shifted to a higher energy (near the location of $SW-He^{2+}$ ions). This is in contrast with the zero-thickness shell case that exhibited a relatively flat subspectrum in the middle-energy range. These differences require further investigation, which is beyond the scope of the present paper.

(3) The distinction between incoming and backstreaming $PUI-H^+$ subspectra is much clearer in the high-energy range, and a similar improvement distinguishing between backstreaming $PUI-H^+$ and backstreaming $PUI-He^+$ ions results in a better agreement between observations and simulation results.

(4) The smaller cutoff for backstreaming $PUI-H^+$ shows that the high-energy range of backstreaming PUIs (within the gray area in Figure 4(d)) is shrunk for the filled-in shell compared with the zero-thickness shell case, i.e., the energization is more limited.

(5) A surprising result is the impact that a filled-shell $PUI-H^+$ distribution has on both SW ion populations. Both exhibit a cooler distribution at $t = 150 \Omega_{ci}^{-1}$ (the width of each distribution decreases for the filled-in shell case), compared with the zero-thickness shell case.

(6) The cutoff “c4” of the highest-energy ions (backstreaming $PUI-He^+$) is unaffected by a filled $PUI-H^+$ shell distribution. These combined effects lead to a relatively flat high-energy tail in the highest-energy range of the spectra, which is consistent with previous observations (McComas et al. 2017; Zirnstein et al. 2018).

Moreover, simulations have been also performed in the case where both PUI populations (H^+ and He^+) are initially described as filled-in shells. A few differences can be noticed in the corresponding spectra shown Figures 4(e) and (f) with respect to the zero-thickness shell case (Figures 4(a) and (b)): (i) as expected, the shoulder in the high-energy range of $PUI-He^+$ is much smoother at $t = 0$; (ii) the percentage of backstreaming $PUI-He^+$ is much lower (Figure 4(f)); (iii) the high-energy range covered by the backstreaming PUI (gray area covered by both $PUI-H^+$ and $PUI-He^+$) is almost unaffected; (iv) the transition between middle- (pink area) and high-energy (gray area) range is smoother; (v) in the middle-energy range, the subspectrum of incoming $PUI-H^+$ presents a peak corresponding to the peak of $SWI-H^+$ population; a similar result is also observed between the peaks of incoming $PUI-H^+$ and $SWI-He^{2+}$.

In summary, by considering a filled-in rather than a zero-thickness shell for $PUI-H^+$, we find that the spectral energy distribution changes quite extensively, especially in the contributions of the different populations within the global or total energy spectrum.

3.3. Impact of Shock Front Obliquity

A comparison between the phase space of the different ion populations (Figure 2) and the associated energy spectra (Figure 3) shows that the reflected ions backstreaming far upstream from the front (selected in the sampling area shown in Figure 2) are energetically important, and are a key component of the highest-energy spectral regime. This implies that shock front obliquity has a significant impact in determining the energetic part of the spectrum. To properly evaluate the importance of shock obliquity to the high-energy part of the spectrum, we undertook a separate simulation for a strictly 90° IP shock. All other plasma and shock conditions remain unchanged; in particular, zero-thickness shells were used for PUIs as for the reference run (Figure 2). For the 90° case, reflected ions can only accumulate over a short distance from the ramp, i.e., in the foot of the perpendicular shock, as under

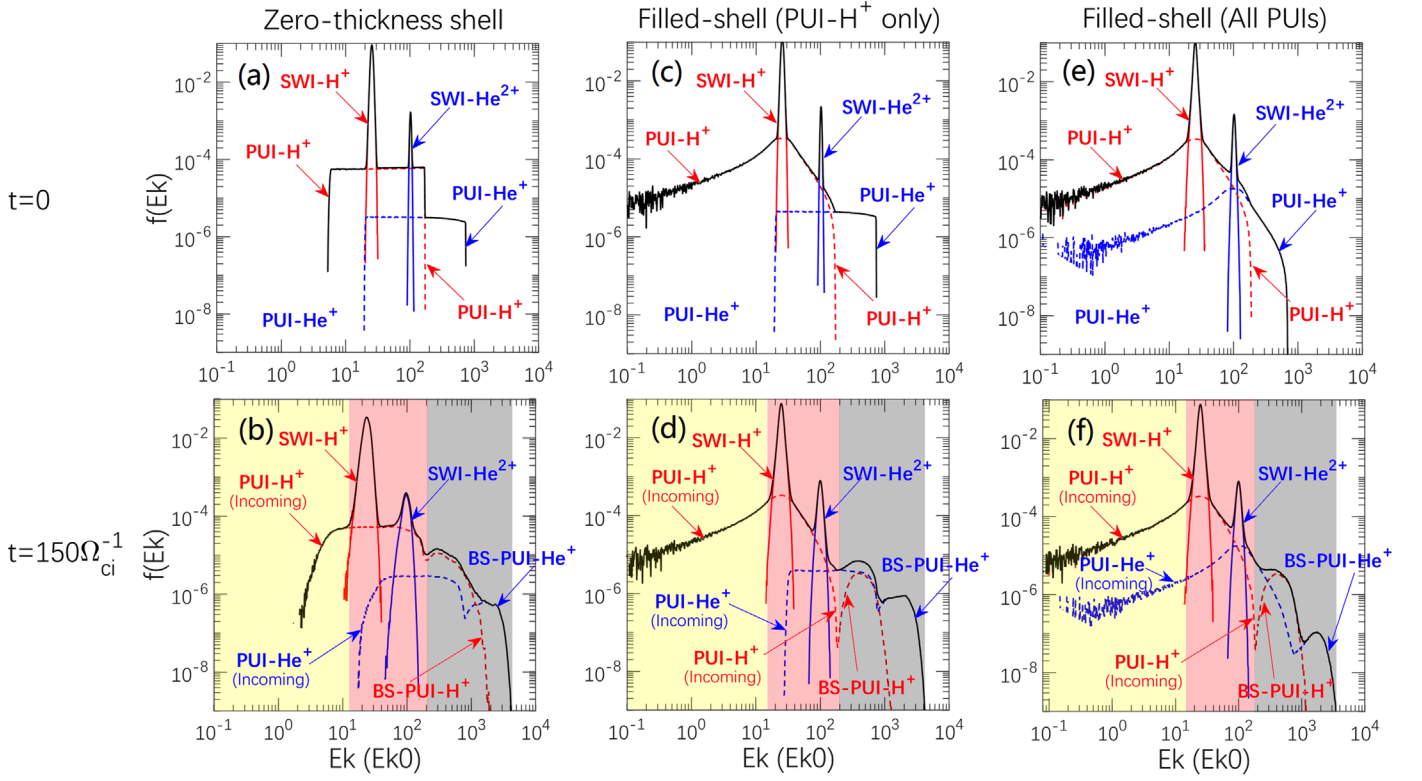


Figure 4. Energy spectrum derived from an initially zero-thickness shell used for both PUI distributions at (a) $t = 0$ and (b) at the late time $t = 150 \Omega_{ci}^{-1}$ of the simulation. Corresponding spectra are shown as an initially filled-shell distribution is used for PUI- H^+ distribution only (plots (c) and (d)), and for both PUI- H^+ and PUI- He^+ distributions (plots (e) and (f)). The red and blue colored curves denote H^+ and heavy ions (He^+ and He^{2+}), respectively; the black curve is used for the global spectrum. The same scales are used for all spectra.

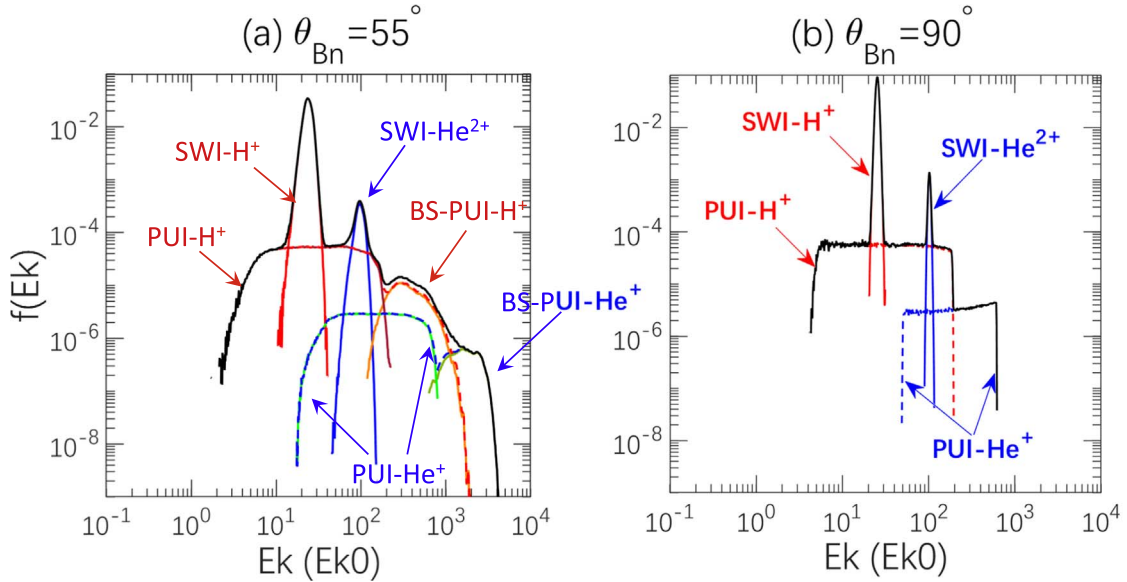


Figure 5. Energy spectra determined upstream of the interplanetary shock with obliquity (a) $\theta_{Bn} = 55^\circ$, and (b) 90° at the same late time $t = 150 \Omega_{ci}^{-1}$ for each simulation. Spectra are derived within the sampling x -range $\Delta x = 300 c/\omega_{pi}$ located at $20 c/\omega_{pi}$ from the ramp for (a), and within a restricted sampling x -range $\Delta x = 15 c/\omega_{pi}$ (as the area of reflected-gyrating ions is quite restricted) located at $15 c/\omega_{pi}$ from the ramp for (b) (see text for further discussion). Red and blue colored curves denote H^+ and heavy ions (He^+ and He^{2+}), respectively; black curve is used for the global spectrum. The same scales are used for both spectra.

the effect of the magnetic field the PUIs are forced to gyrate and return to the front. Consequently, no backstreaming ions can escape upstream from the ramp. Corresponding spectra obtained for 55° and 90° shocks are compared and shown in Figure 5. The main features can be summarized as follows:

(1) As expected, the overall range of particle energies for the 55° shock is much larger than for the 90° shock, which confirms that the high-energy part of the spectrum is due primarily to both backstreaming PUI- H^+ and backstreaming PUI- He^+ .

(2) The spectrum of each PUI population exhibits a plateau (corresponding to the zero-thickness shell of PUIs) with abrupt limits in contrast to the smooth shoulders present for 55° shock case.

(3) The energy range of SW-H^+ and of SW-He^{2+} ions is much smaller for the 90° shock than for the 55° case. This is because, for the 55° case, the backstreaming PUIs/incoming populations interact, leading to the development of a two-stream type instability. The instability affects all particle populations incident on the shock, as illustrated by the modulations in phase space of not only PUIs but also SW electrons and of SW ions (Figure 2). Hence, both PUI and SW ion populations experience some heating due to the instabilities generated by the backstreaming PUI populations. For the 90° shock, the Maxwellian SW ion distribution corresponds to the pristine solar wind only and is unaffected far upstream of the shock front because there are no instabilities triggered by backstreaming ions.

4. Discussion and Conclusions

The work presented here was stimulated by the first direct observations of the mediation and preferential heating of nonthermal PUIs rather than thermal SW ions upstream of an interplanetary shock in the environment of Pluto. To our knowledge, this study is one of the first attempt to understand these recent measurements using self-consistent plasma simulations. Although the simulations presented herein are 1D, they can reproduce the most prominent features of the observed ion energy spectra. These observations were made by the SWAP experiment on the *New Horizons* mission at a distance of 34 au from the Sun (Zirnstein et al. 2018). At this distance, PUI-H^+ is only a few percent of the total proton density, but it contains most of the internal particle pressure (see Zank et al. 2018). Moreover, the observed energy spectra are very similar to those observed at a distance of 22–38 au by SWAP (McComas et al. 2017).

The results presented here show (i) how different parts of the total or global spectrum observed upstream of an IP shock can be understood in terms of the contributions from the different populations (essentially forming subspectra) and (ii) how certain parameters influence these different “subspectra,” allowing us to refine the comparison between observations and simulation results. The simulation results reflect a self-consistent approach and account for the time/spatial scales of all populations. Results presented herein describe the upstream region of an interplanetary shock only, and will be extended to the downstream region in a subsequent analysis. Our primary results can be summarized as follows:

(a) Shock obliquity plays a key role in the formation of energetic PUIs streaming back far upstream from the shock ramp. No backstreaming SW ions are observed.

(b) The “strategy” used herein differs from previous analyses. Instead of fitting different charged particle populations with modeled distribution functions (e.g., Zank et al. 2010), we decomposed the total energy spectrum into three energy ranges, i.e., low-, middle- and high-energy ranges. The three energy ranges correspond, respectively, to (1) incident PUI-H^+ mainly; (2) both SW-H^+ and SW-He^{2+} ions that are superimposed on incident PUI-H^+ population; and (3) both backstreaming PUI-H^+ and backstreaming PUI-He^+ . We emphasize that the backstreaming PUI populations account quite well for the highest-energy part of spectrum above the

incoming PUI-H^+ cutoff. Three other cutoffs can be identified at higher energies: (i) one for incoming PUI-He^+ , (ii) one for backstreaming PUIs-H^+ , and (iii) one for backstreaming PUI-He^+ . This approach allowed us to determine which part of the spectra (and the corresponding subpopulation) is primarily sensitive to various upstream plasma conditions.

(c) When a filled-shell distribution (rather than a zero-thickness shell) is used to describe both the initial PUI-H^+ and PUI-He^+ populations, a better agreement is observed in the low- and high-energy ranges between observational and simulations results. This is important in that it confirms that PUIs do have sufficient time to diffuse in velocity space after the initial pick-up in the supersonic solar wind. However, there are differences between observations and simulations in the middle-energy range, which requires further investigation.

Observational results presented by McComas et al. (2017) and Zirnstein et al. (2018) exhibit different shapes in the global energy spectra, in particular on the “sharpness” of the shoulders that are present in the high-energy regime that is formed primarily by PUI-H^+ and PUI-He^+ . The results presented here are preliminary and focused on one typical observed spectrum, and further parametric analyses will be explored.

We acknowledge the French Centre National d’Etudes Spatiales (CNES) for its support under APR- W-EEXP/10-01-01-05 et APR-Z-ETP-E-0010/01-01-05. Much of the numerical simulations were done on the IDRIS computer center located at Orsay (near Paris), which we thank for its support (DARI project A0050400295). A part of the computations were performed by Numerical Forecast Modeling R&D and VR System of State Key Laboratory of Space Weather. The research is also partially supported by NFSC under grant Nos. 41574140, 41674168, the Open Research Program Key laboratory for the Geospace Environment CAS (GE2017-01), Youth Innovation Promotion Association Funding No. 2017188, Beijing Municipal Science and Technology Commission (grant No. Z191100004319001), Beijing Municipal Natural Science Foundation No. 1192018, Beijing Excellent Talent Training Project Funding No. 2017000097607G049, and the Strategic Priority Research Program of Chinese Academy of Sciences (grant No. XDA14040404). G.P.Z. acknowledges the partial support of the NSF EPSCoR RII-Track-1 Cooperative Agreement OIA-1655280, an NSF/DOE Partnership in Basic Plasma Science and Engineering via NSF grant PHY-1707247, and NASA grant/subaward 0000167 (NNX17AB04G). Z.Y. thanks LATMOS for its nice hospitality during his stay.

ORCID iDs

Bertrand Lembége  <https://orcid.org/0000-0002-5528-0228>
Zhongwei Yang  <https://orcid.org/0000-0002-1509-1529>
Gary P Zank  <https://orcid.org/0000-0002-4642-6192>

References

- Arber, T. D., Bennett, T. D., Brady, C. S., et al. 2015, *PPCF*, **57**, 113001
- Burrows, R. H., Zank, G. P., Webb, G. M., Burlaga, L. F., & Ness, N. F. 2010, *ApJ*, **715**, 1109
- Elliott, H. A., McComas, D. J., Valek, P., et al. 2016, *ApJS*, **223**, 19
- Kumar, R., Zirnstein, E. J., & Spikovsky, A. 2018, *ApJ*, **860**, 156
- Lee, R. E., Chapman, S. C., & Dendy, R. O. 2005, *AnGeo*, **23**, 643
- Lembége, B., & Yang, Z. W. 2016, *ApJ*, **827**, 73
- Lembége, B., & Yang, Z. W. 2018, *ApJ*, **860**, 84
- Lipatov, A. S., & Zank, G. P. 1999, *PRL*, **84**, 3609

- Matsukiyo, S., & Scholer, M. 2011, [JGR](#), **116**, A08106
- Matsukiyo, S., Scholer, M., & Burgess, D. 2007, [AnGeo](#), **25**, 283
- McComas, D., Allegrini, F., Bagenal, F., et al. 2008, [SSRv](#), **140**, 261
- McComas, D. J., Zirnstein, E. J., Bzowski, M., et al. 2017, [ApJS](#), **233**, 8
- Oka, M., Zank, G. P., Burrows, R. H., & Shinohara, I. 2011, in AIP Conf. Proc. 1366, Partially Ionized Plasmas throughout the Cosmos—Proceedings of the 2010 Huntsville Workshop, ed. V. Florinski, J. Heerikhuisen, & G. P. Zank (Melville, NY: AIP), 53
- Vasyliunas, V. M., & Siscoe, G. L. 1976, [JGR](#), **81**, 1247
- Williams, L. L., & Zank, G. P. 1994, [JGR](#), **99**, 19229
- Yang, Z. W., Han, D. S., Yang, H. G., et al. 2012a, [Ap&SS](#), **341**, 241
- Yang, Z. W., Lembege, B., & Lu, Q. M. 2012b, [JGR](#), **117**, A07222
- Yang, Z. W., Liu, Y. D., Richardson, J. D., et al. 2015, [ApJ](#), **809**, 28
- Zank, G. P. 1999, [SSRv](#), **89**, 413
- Zank, G. P. 2015, [ARA&A](#), **53**, 449
- Zank, G. P., Adhikari, L., Zhao, L.-L., et al. 2018, [ApJ](#), **869**, 23
- Zank, G. P., Heerikhuisen, J., Pogorelov, N. V., Burrows, R., & McComas, D. 2010, [ApJ](#), **708**, 1092
- Zank, G. P., Pauls, H. L., Cairns, I. H., & Webb, G. M. 1996, [JGR](#), **101**, 457
- Zhao, L.-L., Zank, G. P., & Adhikari, L. 2019, [ApJ](#), **879**, 32
- Zirnstein, E. J., McComas, D. J., Kumar, R., et al. 2018, [PvRvL](#), **121**, 075102